Noninvasive Imaging of Molecular Dynamics in Heterogeneous Materials

Rohit Bhargava and Ira W. Levin*

Laboratory of Chemical Physics, National Institute of Diabetes and Digestive and Kidney Diseases, National Institutes of Health, Bethesda, Maryland 20892-0510

Received August 15, 2002

ABSTRACT: The macroscopic properties of microscopically heterogeneous materials are often determined by specific molecular changes within constitutive microdomains. In particular, the electrooptical properties of a class of composites termed polymer-dispersed liquid crystals (PDLCs) are established by the orientation dynamics of the component liquid crystals (LCs) and the dissolved species dictated by applied electric fields. We demonstrate the accessibility of spatially resolved molecular dynamics in the millisecond time regime by developing a time-resolved Fourier transform infrared (FTIR) spectroscopic imaging technique. Applying this approach to PDLCs, we determine the molecular reorientation dynamics to be a strong function of spatial position. The liquid crystal and polymer segmental dynamics correlate through dipole−dipole interactions, demonstrating that chemical factors other than surface anchoring interactions contribute significantly to the electrooptical characteristics of polymer−LC composites. The morphologically specific dynamics and molecular interactions are determined noninvasively and without addition of foreign materials or molecular labeling.

Introduction

PDLCs,[1,2] or dispersions of low molecular weight LC microdomains within a polymeric matrix, provide alternative materials for electrooptical devices[3−7] because of both the sensitivity of their light scattering properties to applied electrical potential differences and their favorable physical properties.[8] While the macroscopic light transmission characteristics of these systems have been extensively studied,[9] the localized molecular dynamics that determine this behavior are not well understood. A direct observation of molecular orientation is most useful in understanding this phenomenon. Nuclear magnetic resonance (NMR), Fourier transform infrared (FTIR), and Raman spectroscopic techniques that allow macroscopic observations of segmental motion are particularly attractive. However, techniques to characterize the site-specific LC dynamics in PDLCs require both chemical specificity and spatial resolution. As spectroscopic techniques were largely unable to satisfy the dual criteria, experimental attempts to visualize localized segmental dynamics using optical methods have relied on the incorporation of dyes,[10] which affect the system dynamics,[11] have involved neat liquid crystals,[12] which do not adequately simulate the encapsulated state, or have applied near-field techniques,[13,14] which are invasive.

IR spectroscopy provides a noninvasive determination of molecular composition, conformation, and orientation, in addition to identifying specific molecular interactions.[15] Dynamic processes have also been monitored using fast real-time and time-resolved spectroscopic techniques. While IR spectroscopic microscopy has been accessible for over 50 years[16] for the localized characterization of heterogeneous materials, the recent coupling of interferometry and focal plane array (FPA) detectors[17] has increased the versatility of the technique toward allowing rapid, spatially resolved measurements.[18] In this paper, we develop an imaging technique, conceptualized in Figure 1 and detailed in the Experimental Section, for analyzing repetitive dynamic phenomena on the millisecond time scale while retaining the critical chemical specificity and spatial selectivity of FTIR imaging.

Experimental Section

Instrumentation. The time-resolved infrared spectroscopic imaging technique involves the use of a step-scan infrared interferometer coupled to a microscope equipped with a two-dimensional FPA detector as in the standard FTIR imaging configuration.[17] As shown in Figure 1, the interferometer mirror was rapidly moved to a stable optical retardation. For each optical retardation, the dynamic phenomenon was initiated, and the resulting infrared intensity was recorded as a function of time. This process was repeated until the entire interferogram was acquired. Since the radiation intensity at each optical retardation was acquired over the field of view of the array detector at different times, an interferogram was obtained that corresponds to each detector pixel or to a specific spatial area on the sample and was temporally unique with respect to the initiation of the dynamic event. The instrumentation was constructed using a commercially available step-scan spectrometer (Bruker Optics, IFS-66/s), an infrared microscope (Bruker IR Scope II), and a mercury cadmium telluride (MCT) FPA (Santa Barbara Focalplane, CA). The microscope employed reflective Cassegranian optics for focusing the beam onto the sample plane and subsequent direction to the FPA, which was equipped with an appropriate cold shield and optical filters. All experiments were carried out in a transmittance mode. A 15× objective was used to the image a sample area field of view (∼750 μm × 750 μm) onto the 256 × 256 pixel FPA. A single interferogram was acquired for every pixel corresponding to each time resolution element. The time required for trigger pulses was 1 μs, which is negligible compared to other times in the collection process. Event-locked signal generators (Agilent Inc.) were employed to initiate the experiment and data collection. A commercial amplifier (Krohn-Hite Corp.) was employed to increase the electric potential difference generated between 1 and 5 V at 1 kHz and applied to the PDLC.

Sample. The PDLC studied was a dispersion of the commonly used liquid crystal eutectic mixture, E7 (EM Industries, Inc.) in a photocured NOA65 (Norland Optical Adhesive Inc.)

* To whom correspondence should be addressed.

10.1021/ma021336r
Published on Web 12/02/2002

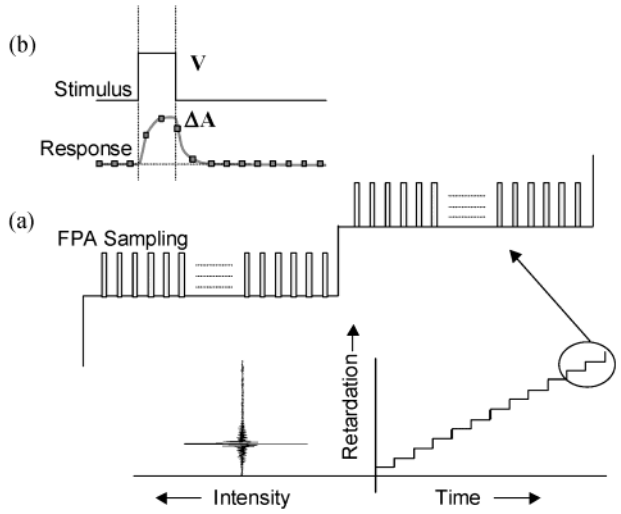

Figure 1. (a) An interferogram for each pixel on an FPA detector is acquired by obtaining the radiation intensity as a function of retardation in a step-scan manner. (b) For each retardation, the PDLC is subjected to a 2 kHz ac electric potential difference, *V*, for 100 ms at a time period of 65 ms after beginning the observation. Voltages of 5, 10, 15, 20 and 30 V were employed. The response is sampled for 70 μs after every 10 ms for a total time period of 2.5 s per excitation. The sample is excited once per retardation step.

matrix. E7 consists of 51% *n*-pentylcyanobiphenyl (5CB), 25% *n*-heptylcyanobiphenyl (7CB), 16% *n*-octyloxycyanobiphenyl (8OCB), and 8% *n*-penyltcyanoterphenyl (5CT). The nematic−isotropic transition temperature of this system was reported to be about 333 K; a smectic-to-nematic and a glass transition occurred about 243 and 213 K, respectively. The polymeric matrix, NOA65, was reported to be a mixture composed primarily of trimethylolpropane diallyl ether, trimethylolpropane tris thiol, isophorone diisocyanate ester, and a benzophenone photoinitiator.[19] All materials were used as received. Weight ratios (65% LC) of the two components were intimately mixed by hand at 350 K, a temperature above the nematic-to-isotropic transition of the LC. A small amount of the solution was sandwiched between indium tin oxide (ITO)-coated CaF_2 plates separated by 10 μm diameter cylindrical spacers and photocured[20] using a long wave UV lamp (UVP Inc.) after maintaining the sample for 4 h at a low temperature (−5 °C), as detailed elsewhere.[22]

Data Collection and Processing. Data were collected over the mid-infrared region (0−3950 cm^{-1}) by sampling the interferogram at every fourth zero crossing of the He−Ne reference laser. The interferogram data set consisted of 1024 data points, resulting in a spectral resolution of 8 cm^{-1}. A total of 250 temporal sampling points were collected in sequence for each retardation step, 10 ms apart, resulting in a total of 256 000 data points per pixel. An additional 1.5 s is provided per step to allow for complete molecular relaxation, resulting in a total time per retardation step of 4 s. The data sets were spatially partitioned to a quarter of the acquired data set to reduce file sizes. Prior to data acquisition, the focal-plane array was flat-fielded at low intensity. Individual interferogram cubes were extracted from the data sets and fast Fourier transformed using triangular apodization and a fill factor of 4 to produce single-beam images. All data acquisition and processing were carried out using custom developed software. Further details on instrumentation and data processing can be found elsewhere.[21]

Results and Discussion

The observed morphology of a PDLC using optical microscopy is shown in Figure 2a. Under crossed polarizers (Figure 2b), optical patterns arising from the local organization of LC molecules within domains are detected. Most droplets exhibit bipolar configurations including two point defects, and as a consequence of the film's thinness, their symmetry axis lies in the plane of the film. Simultaneously determined chemical and morphological information on the microscopic structures of PDLCs obtained by FTIR imaging[22] is shown in Figure 2c,d. These images reveal the distribution of the chemical species representative of the liquid crystal and the polymer, respectively, demonstrating that the liquid crystalline domains retain a small concentration of dissolved polymer, while the polymer-rich matrix contains dissolved LCs. The dissolved matrix material is believed to lower the nematic−isotropic transition temperature, induce defects, and degrade optical properties.[23] However, the mechanism of these effects remains unclear. While the domain organization and the resulting optical patterns are caused by packing of the rodlike nematic LC in cavities, as shown in Figure 2e, a comparison of the chemical and polarized microscopy images reveals that the occurrence of the atypical maltese cross pattern is caused by presence of dissolved polymer in the LC domain. Since macroscopic light scattering and dielectric spectroscopic studies of the composites vary considerably with different droplet configurations,[24] vibrational spectroscopic imaging provides an informative chemical basis for understanding morphological characteristics.

In the quiescent state, a refractive index mismatch at LC domain boundaries serves to scatter radiation, leading to the opacity of the PDLC film. When an electric field is applied, individual liquid crystal molecules orient along the propagation vector of the electric field,[25] as shown in Figure 2f. Additionally, point defects in the domain move from the equatorial to the axial plane. Since the refractive index of the liquid crystal is anisotropic, the refractive index of the aligned liquid crystal and the polymer are chosen such that their refractive indices are equal in the viewing direction. Thus, the dynamic response of LC molecules to electrical stimulation determines the light modulation properties of devices incorporating PDLCs. Although various optical and dielectric spectroscopic techniques are used to examine a film's average behavior, they have no spatial resolution and poor chemical sensitivity. Recent examinations using near-field scanning optical microscopy (NSOM) show promise for delineating the microscopic behavior, but this approach involves excitation of only a small portion of the PDLC resulting in significant confinement effects[26] and has no chemical sensitivity. Nuclear magnetic resonance (NMR) techniques are chemically specific but present inherent spatial resolution limitations.[27] Hence, a spatially resolved dynamic response of PDLCs that includes information on individual molecular orientation and interactions has not been generally accessible. The average molecular dynamics of neat LCs[28,29] and a PDLC[30,31] have been examined using single detector time-resolved IR spectroscopy. As opposed to these studies of bulk liquid crystal, the LC in a PDLC resides in several different local environments and is subject to additional constraints from domain boundaries and defects. To date, there are no reported studies describing morphologically specific LC dynamics in distinct regions of either the droplet or the interface.

The response of an LC domain in the PDLC subjected to an electrical stimulus, as described in Figure 1, is shown in Figure 3a. As the LC is aligned perpendicular

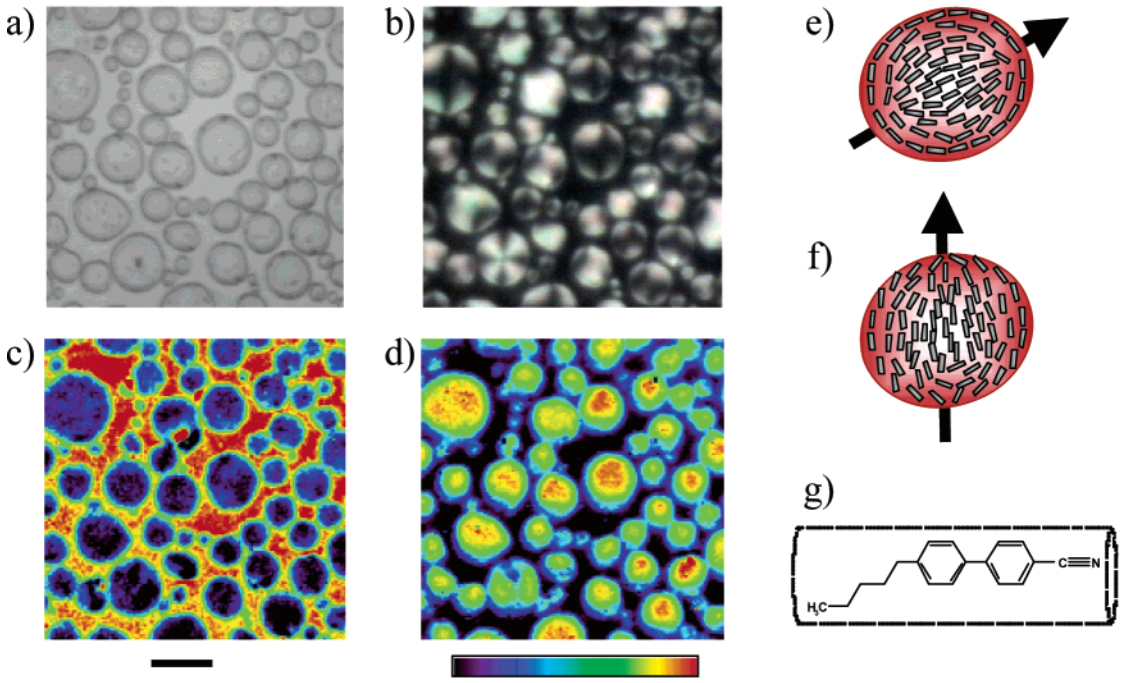

Figure 2. Liquid crystalline domains in a polymer-rich matrix examined (a) using optical microscopy and (b) under cross polarizers. The absorbance distribution (c) of the C≡N stretching mode specific to the liquid crystal and (d) of the C═O stretching mode specific to the polymer as obtained from FTIR imaging. The color bar indicates low concentration (blue) to high concentration (red). The size bar is 100 μm. (e) A typical LC-rich domain contains oriented LC molecules with the average director as shown. (f) Upon application of the electric field, individual molecules reorient along the direction of the field. (g) The nematic LC is a rodlike molecule.

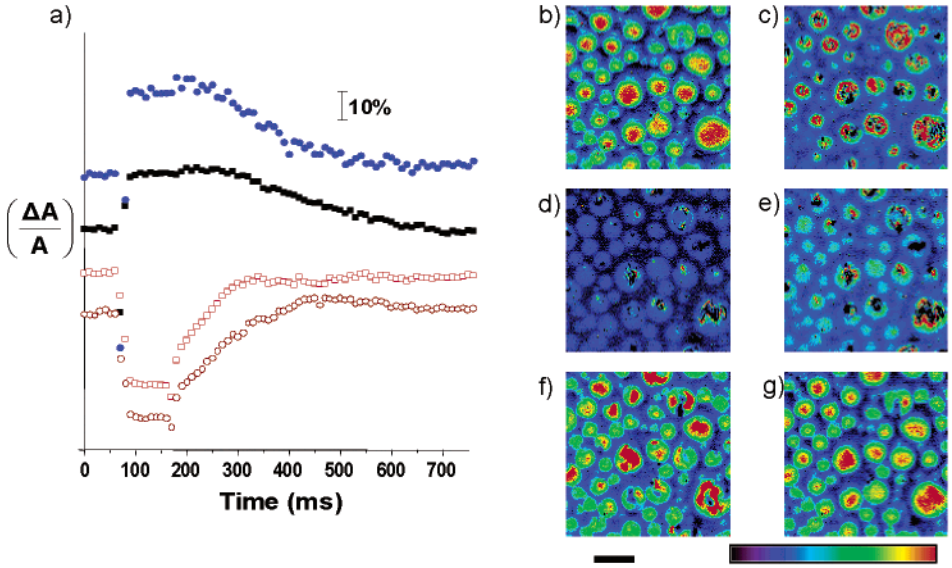

Figure 3. (a) Plots of the temporal variation of signals for C≡N stretching (open squares) and C−C stretching vibrations (open circles) specific to the liquid crystal, the C═O vibrational mode (filled squares) specific to the polymer, and the CH_3 antisymmetric stretching modes of both the polymer and the liquid crystal. The absorbance distribution of the nitrile group specific to the liquid crystal is shown at (b) 0 ms, (c) 80 ms, (d) 160 ms, (e) 200 ms, (f) 500 ms, and (g) 1.5 s for 20 V potential differences. The color bar intensity limits are 0.25 and 0.65; the size bar corresponds to 100 μm.

to the electric field of the propagating infrared radiation, the absorbance of molecular moieties oriented along the molecule's major axis decreases, since the absorbance is proportional to the square of scalar product of the transition dipole moment and the electric field vector. The nitrile (C≡N) moiety dipole is rigidly aligned along the major axis of the molecule and is, therefore, representative of molecular orientation. As the electric field is applied, absorbance decreases and, upon removal of the field, the absorbance increases, corresponding to molecular reorientation and relaxation processes, respectively. The temporal response of some constituent functional groups of the chemical components is shown in Figure 3b. The polymer-specific carbonyl (C═O) group aligns perpendicularly to the nitrile group in this domain as indicated by the increase in absorbance upon application of the electric field. Similarly, the C−C stretching vibrational mode is aligned along the same axis as the nitrile stretching mode and demonstrates the same behavior as the nitrile stretching vibration.

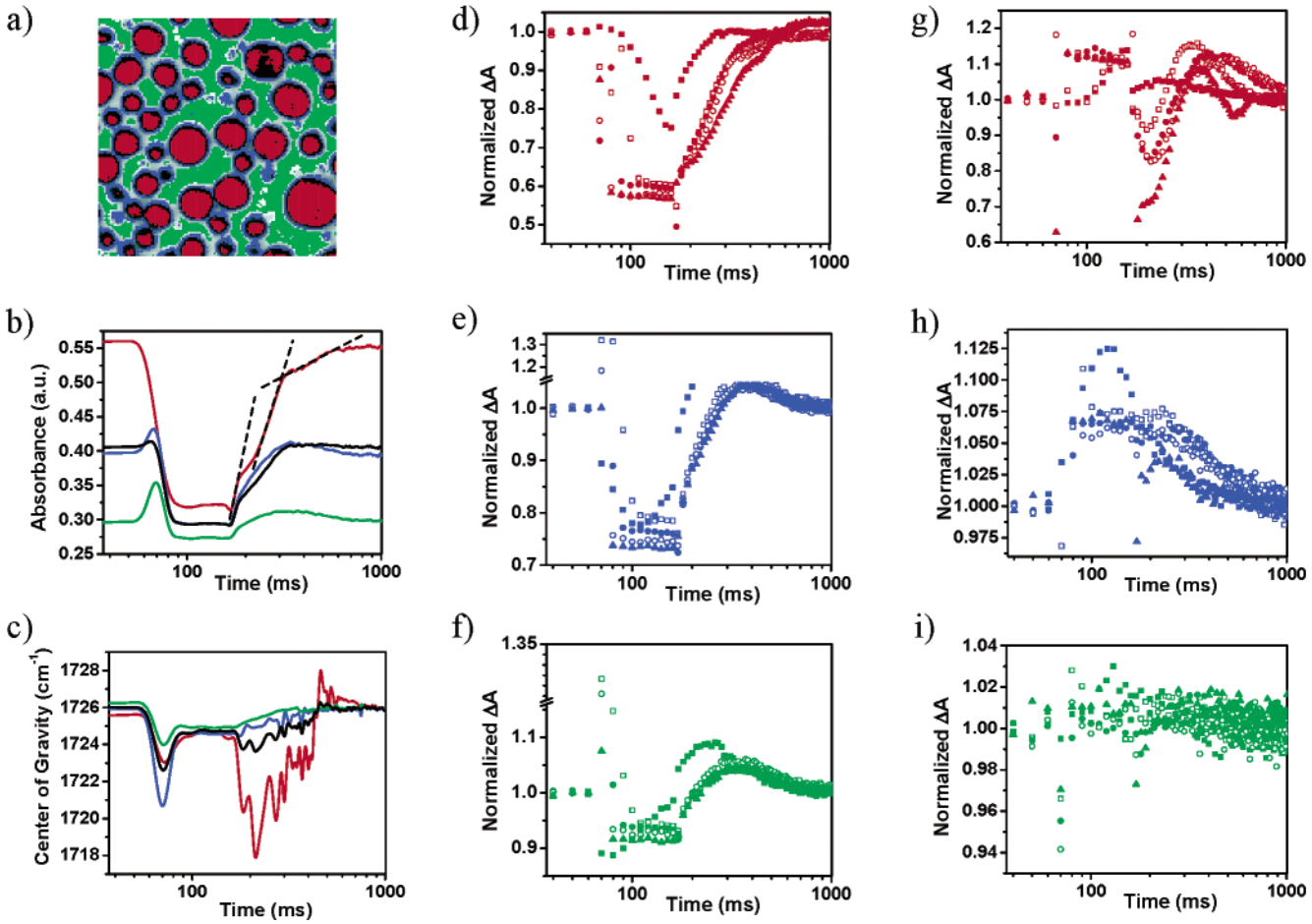

Figure 4. (a) LC-rich domains, matrix, and interface-rich regions are delineated as red, green, and blue, respectively. The red, blue, and green colors in the plots from (b) through (i) correspond to the average time profiles of the regions. (b) Nitrile stretching absorbance of the three regions at 20 V. (c) Center of gravity of the carbonyl peak for 20 V. (d−f) Nitrile stretching and (g−i) carbonyl stretching modes display the response as a function of applied voltages of 5 V (filled squares), 10 V (hollow squares), 15 V (filled circles), 20 V (hollow circles), and 30 V (filled triangles).

The CH_3 vibrational mode contains contributions from both the liquid crystal and the polymer. While the two responses cannot be separated on the basis of the absorbance of this mode alone, the net absorbance change indicates that the vibrational mode is orthogonally aligned to the major axis of the LC molecule. The variation in absorbance of the nitrile group as a function of time over the entire field of view is shown in Figure 3b−g. Since the elastic free energy density is significantly lower for large droplets whose centers are in contact with the electrodes, multiple defect structures are formed. These defect structures evolve during the course of molecular reorientation and relaxation. Thus, the essential chemical and morphological features are readily captured by millisecond time-resolved FTIR imaging.

Characteristic molecular dynamics indicated by the absorbance of the nitrile group for different PDLC regions, as delineated in Figure 4a, are shown in Figure 4b for a 20 V excitation. While the orientation is rapid, the relaxation of the bulk droplet regions consists of three factors as opposed to the two commonly assumed relaxation processes dictated by boundary anchoring and bulk relaxation. The presence of three processes is indicated by three exponentially decaying relaxations in the time profiles indicated by dashed lines in Figure 4b. Molecules located close to the droplet boundary experience the strongest anchoring and, thus, the greatest restraining and restoring forces. The boundary region also exhibits the maximum refractive index difference between the phases; consequently, molecules in this region dominate the light scattering behavior of a PDLC. Upon application of the electric field, the response of the boundary-rich region shows an increase in absorbance prior to a decrease indicative of reorientation. This absorbance increase arises when molecular dipoles originally oriented below the equatorial plane pass through the equatorial plane as a consequence of the rotating torque from the vector product of the electric field and the LC dipole. The absence of this absorbance increase prior to reorientation for the droplet bulk phase indicates an alignment of the bulk molecules in the equatorial plane. Since molecular relaxation is slower, a broad increase above the quiescent absorbance is observed for the boundary regions prior to the absorbance returning to the quiescent value. A relatively larger effect is observed for the matrix where half the randomly oriented molecules are expected to be oriented below the equatorial plane. The average response denoted by the black curve in Figure 4b, which would be observed using bulk experimental methods,[32] may not reveal these details. The behavior of each region can be seen as a function of applied voltage in Figure 4d−f.

We note that the center of gravity of the carbonyl peak, which is sensitive to dipole−dipole interactions,

changes as shown in Figure 4c. Universally, it can be seen that the polymer−LC interaction serves initially to retard the reorientation, as evidenced by an increase in interaction manifest in the shift to lower wavenumber of the carbonyl stretching mode (for example, from 1726 to 1721 cm^{-1} at the boundary). As this interaction is lost, the carbonyl group relaxes into the equatorial plane in the volume vacated by the oriented LC molecule, as observed by the carbonyl group dynamics in Figure 4g−i. The carbonyl group and LC relaxation are again strongly coupled as the electric field is removed. Since the coupling persists for a longer time period than the LC relaxation process, the hysteresis effects observed in PDLCs[25,33,34] can be explained. The relative behavior of the polymer and the LC is described as a function of applied voltage in Figure 4d−i. This is the first report and, to the best of our knowledge, the only method available for directly determining molecular dynamics and interactions of a dissolved material in LC droplets. Although it is recognized that the dynamics of LC molecules are influenced by the viscosity of the liquid crystalline phase, elasticity of the LC molecules and the defects, and shapes and sizes of the dispersed phase, the above results indicate that both the LC dynamics coupled to the dynamics of the dissolved polymer and their specific interactions play a major role in explaining the properties of this class of materials.

Conclusions

Over the past two decades, new imaging methods and chemically specific techniques that monitor dynamics have been separately developed. We believe that the current work addresses both areas by providing chemically sensitive measurements of *spatially resolved dynamics*. In contrast to techniques that employ limited spectral range lasers for fast dynamics, our method provides the entire mid-infrared spectrum for molecular analyses; in contrast to single detector subsecond FTIR spectroscopy, our imaging technique provides observations at thousands of spatially specific locations. For the class of electrooptical materials that we examine in this paper, the observed dynamics are functions of both spatial location and intermolecular coupling. The latter cannot be determined by any other technique that simultaneously allows spatially resolved measurements. These results are, for example, relevant specifically to the design and performance of liquid crystal devices. Similar insights, however, accrued from time-resolved spectroscopic imaging will lead to enhanced understandings of the functional characteristics of molecular systems spanning the materials and biological disciplines.

References and Notes

(1) Doane, J. W.; Vaz, N. A.; Wu, B. G.; Zumer, S. *Appl. Phys. Lett.* **1986**, *48*, 269−271.
(2) Drzaic, P. S. In *Liquid Crystal Dispersions*; World Scientific: Singapore, 1995.
(3) West, J. L. *Mol. Cryst. Liq. Cryst.* **1988**, *157*, 427−441.
(4) Doane, J. W. In *Liquid C*rystals−*A*pplications and *U*ses; Bahadur, B., Ed.; World Scientific Publishing: Singapore, 1990; Vol. 1.
(5) Blanca, C. M.; Gutierrez, R. C.; Domingo, Z. B. *Mol. Cryst. Liq. Cryst.* **2001**, *368*, 4023−4030.
(6) Chidichimo, G.; Formoso, P.; Manfredi, S.; Favaro, G.; Mazzucato, U.; Romani, A. *J. Appl. Phys.* **2001**, *90*, 4906−4914.
(7) Lucchetta, D. E.; Manni, A.; Karapinar, R.; Gobbi, L.; Simoni, F. *Mol. Cryst. Liq. Cryst.* **2002**, *375*, 397−409.
(8) Bouteillier, L.; LeBarny, P. *Liq. Cryst.* **1996**, *21*, 157−174.
(9) Aloe, R.; Chidichimo, G.; Golemme, A. *Mol. Cryst. Liq. Cryst.* **1991**, *202*, 9−24.
(10) Higgins, D. A.; Liao, X. M.; Hall, J. E.; Mei, E. W. *J. Phys. Chem. B* **2001**, *105*, 5874−5882.
(11) West, J. L.; Ondris-Crawford, R. *J. Appl. Phys.* **1991**, *70*, 3785−3790.
(12) Snively, C. M.; Koenig, J. L. *J. Mol. Struct.* **2000**, *521*, 121−126.
(13) Mei, E.; Higgins, D. A. *J. Phys. Chem. A* **1998**, *102*, 7558−7563.
(14) Mei, E.; Higgins, D. A. *Appl. Phys. Lett.* **1998**, *73*, 3515−3517.
(15) Lin-Vien, D.; Colthup, N. B.; Fateley, W. G.; Graselli, J. G. *The Handbook of Infrared and Raman Characteristic Frequencies of Molecules*; Academic Press: New York, 1991.
(16) Barer, R.; Cole, A. R. H.; Thompson, H. W. *Nature (London)* **1949**, *163*, 198−201.
(17) Lewis, E. N.; Treado, P. J.; Reeder, R. C.; Story, G. M.; Dowrey, A. E.; Marcott, C.; Levin, I. W. *Anal. Chem.* **1995**, *67*, 3377−3381.
(18) Bhargava, R.; Levin, I. W. *Anal. Chem.* **2001**, *73*, 5157−5167.
(19) Smith, G. W. *Mol. Cryst. Liq. Cryst.* **1991**, *196*, 89−102.
(20) Bhargava, R.; Wang, S.-Q.; Koenig, J. L. *Macromolecules* **1999**, *32*, 8982−8988.
(21) Bhargava, R.; Levin, I. W. *Appl. Spectrosc.*, submitted for publication.
(22) Bhargava, R.; Wang, S.-Q.; Koenig, J. L. *Macromolecules* **1999**, *32*, 2748−2760.
(23) Vaz, N. A.; Smith, G. W.; Montgomery, G. P., Jr. *Mol. Cryst. Liq. Cryst.* **1987**, *146*, 17−34.
(24) Levy, O. *Phys. Rev. E* **2000**, *61*, 5385−5400.
(25) Drzaic, P. S. *Liq. Cryst.* **1988**, *3*, 1543−1559.
(26) Higgins, D. A. *Adv. Mater.* **2000**, *12*, 251−264.
(27) Aloe, R.; Chidichimo, G.; Golemme, A. *Mol. Cryst. Liq. Cryst.* **1991**, *203*, 9−24.
(28) Gregoriou, V. G.; Chao, J. L.; Toriumi, H.; Palmer, R. A. *Chem. Phys. Lett.* **1991**, *179*, 491−496.
(29) Nakano, T.; Yokoyama, T.; Torimui, H. *Appl. Spectrosc.* **1993**, *47*, 1354−1366.
(30) Kohri, S.; Kobayashi, J.; Tahata, S.; Kita, S.; Karino, I.; Yokoyama, T. *Appl. Spectrosc.* **1993**, *47*, 1367−1369.
(31) Snively, C. M.; Chen, P. Y.; Palmer, R. A.; Koenig, J. L. *Mol. Cryst. Liq. Cryst. A* **1996**, *289*, 11−23.
(32) Hasegawa, R.; Sakamoto, M.; Sasaki, H. *Appl. Spectrosc.* **1993**, *47*, 1386−1389.
(33) West, J. L.; Kelly, J. R.; Jewell, K.; Ji, Y. *Appl. Phys. Lett.* **1992**, *60*, 3238−3240.
(34) Yamaguchi, T.; Kawata, Y.; Mori, Y. *Appl. Phys. Lett.* **1998**, *72*, 1170−1172.

MA021336R